Supplementary Materials: Cooling Crystallization with Complex Temperature Profiles on a Quasi-Continuous and Modular Plant

Stefan Höving [1]*[ID]**, Bastian Oldach** [1][ID] **and Norbert Kockmann** [1][ID]

1. Supplementary Information: Experimental Setup

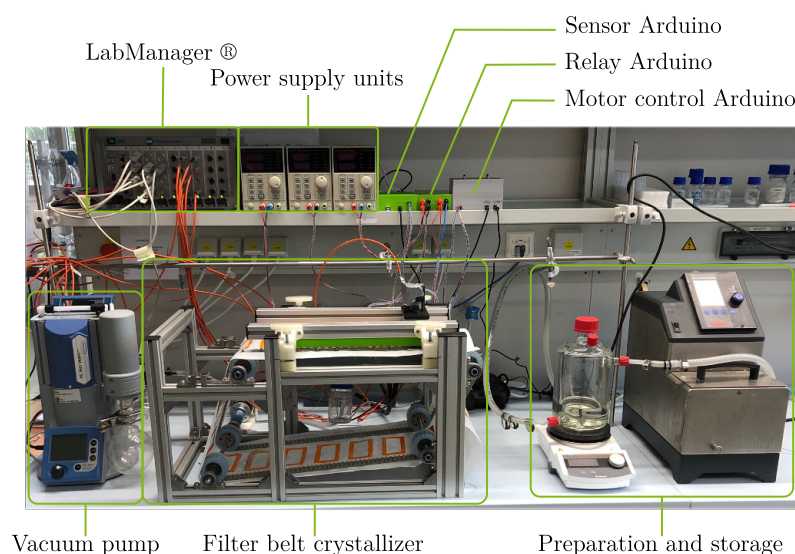**Figure S1.** Complete experimental setup as it was operated in the lab.

2. Supplementary Information: Heating and Cooling Rates

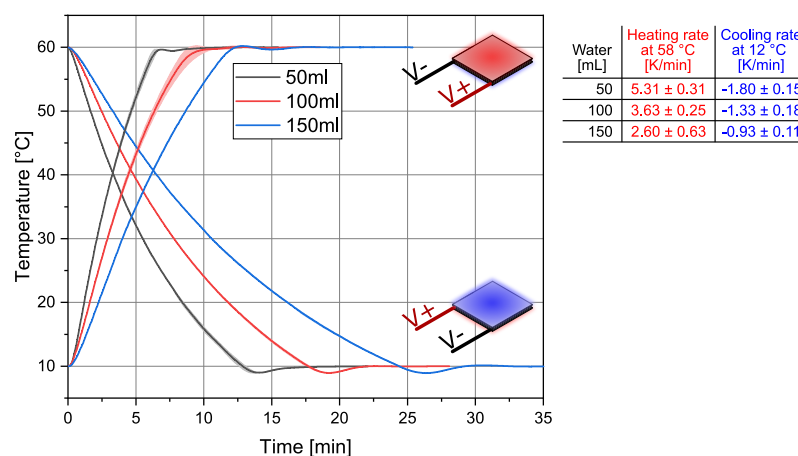| Water [mL]	Heating rate at 58 °C [K/min]	Cooling rate at 12 °C [K/min]
50	5.31 ± 0.31	-1.80 ± 0.15
100	3.63 ± 0.25	-1.33 ± 0.18
150	2.60 ± 0.63	-0.93 ± 0.11

Figure S2. Heating and cooling behavior of different volumes of water in the process container. Cooling and heating rates at 12 °C and 58 °C are given in the table.
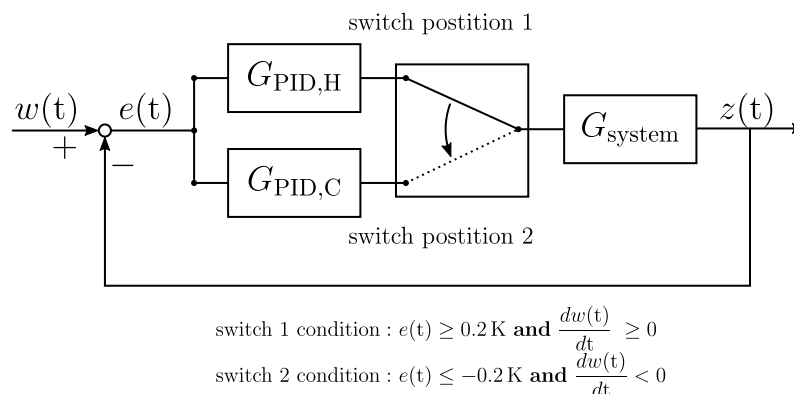
3. Supplementary Information: PID Controller

switch position 1

switch position 2

$$\text{switch 1 condition}: e(\text{t}) \geq 0.2\,\text{K and } \frac{dw(\text{t})}{d\text{t}} \geq 0$$

$$\text{switch 2 condition}: e(\text{t}) \leq -0.2\,\text{K and } \frac{dw(\text{t})}{d\text{t}} < 0$$

Figure S3. Visualization of the temperature control loop with the switching condition between the heating and cooling PID controller.

4. Supplementary Information: Operation Modes

As mentioned before, temperature control can be operated in two different modes. Either the temperature of the aluminum module below the suspension is controlled as it has been done by Dobler *et.al.* and Löbnitz [1,2] (indirect mode), or the temperature in the suspension itself is controlled (direct mode). This is possible due to the temperature sensor and the stirrers being submerged in the suspension. This contribution will demonstrate that both operation modes are possible; however, the focus will be on controlling the suspension temperature.

Figure S4 shows the boxplots of both experimental series. Experimental conditions were standard for both except for their individual temperature control strategy. In **(a)** the temperature of the module was controlled on three temperature modules to mimic the behavior of six modules to increase the resolution from 20 K to 10 K. One can see that the temperature of the stirred suspension converges towards the temperatures of the modules as it is known from natural temperature profiles and as it has been demonstrated by
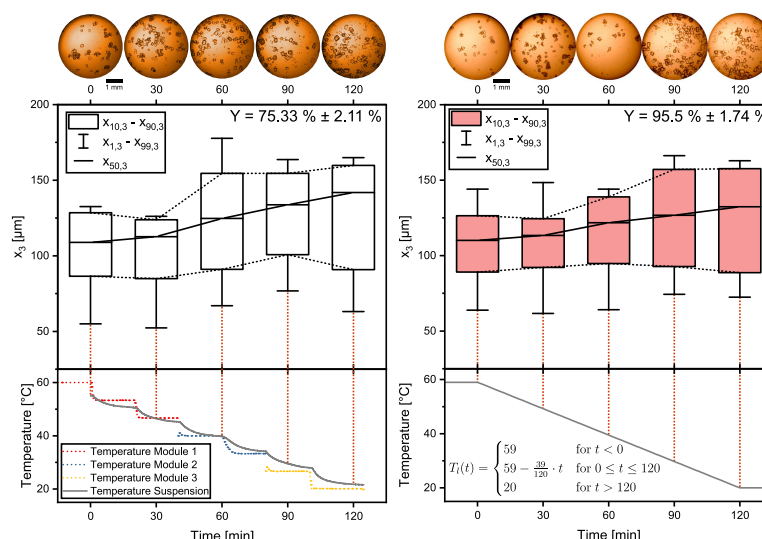

Figure S4. Boxplots of the CSDs at different times for triple experiments of the step-wise temperature profile and the linear temperature profile. Experimental conditions can be red from Table 1. In **(a)** a stepwise temperature profile is carried out across the temperature modules with the indirect temperature control. In **(b)** the temperature of $T_1(t)$ is followed. Yields are indicated in the top right corner. Quantiles are averages of triple experiments. The temperatures are plotted in the bottom panels.

Löbnitz [1] on a comparable apparatus. The temperature profile in b) is also operated on three temperature modules. However, the suspension is temperature-controlled with the control mentioned above strategy to follow a continuous temperature function. The boxplots show that both operation modes start with seed crystals from the same sieve fraction (90-125 µm). In both processes, crystal growth is noticeable while broadening the distribution as it is common for non-ideal crystallization processes [3]. The product crystals in a) come out with a median crystal size $x_{50,3} = 141.9\,\mu m \pm 1.6\,\mu m$ whereas the product crystals of the continuous temperature profile were smaller with $x_{50,3} = 132.4\,\mu m \pm 2.7\,\mu m$. The interquantile range, stays the same for both sets of experiments. From the distributions in Figure S4 there is no benefit of the continuous operation over the step-wise temperature noticeable regarding the $IQR_{90,10}$. Looking at the relative yields of both sets, which are $Y_{steps} = 75.33\,\% \pm 2.11\,\%$ and $Y_1 = 95.5\,\% \pm 1.74\,\%$ one can observe a significant difference. The assumption is that big gradients in the temperature lead to fluctuating supersaturations which in turn affect the crystal growth and, therefore the $Y_{rel.}$. In addition, the temperature of the suspension did not reach the desired 20 °C of the last module, which also affected the $Y_{rel.}$. Due to the effects of the stepwise operation mode, continuous temperature functions as temperature profiles have been used for the following investigations.

5. Supplementary Information: Analytic

The sample washing device is 3D-printed from PLA (polylactic acid) and consists of two equal parts that resemble a tube. They are pressed together and hold a filter cloth (22 µm pore size, SEFAR TETEX® MONO 07-76-SK 022, Sefar AG, Switzerland) and two sealing rings (Figure S5 a)). The filtration area is 50.3 mm². The samples of 0.25 mL taken during the experiments are injected into one side of the device (step 1) (Figure S5 b)). For step 2, pressurized air is applied to the device. It is done as long as it takes until no more mother liquor leaves the bottom side for 20 s. For step 3, the filter cake is washed with 1 mL of 95 % EtOH (VWR International, US) for five times in total. The solubility of sucrose in EtOH of 95 % is $0.0007\,g \cdot g^{-1} \pm 0.0002\,g \cdot g^{-1}$ according to [4] and thus very low. After that, the device is turned upside down, and the filter cake is washed back into the LUMiReader® cuvette that is necessary for the analysis of the volumetric CSD via "Space- and Time-resolved Extinction Profiles" (STEP™) -technology. To validate that the washing device has a negligible influence on the CSD of the product crystals, sucrose crystals of three different sieve fractions (63-90 µm, 90-125 µm, and 125-180 µm) have been investigated. All three fractions have been analyzed directly in ethanol and after being suspended in saturated sucrose (room temperature) with subsequent washing step in triple experiments.
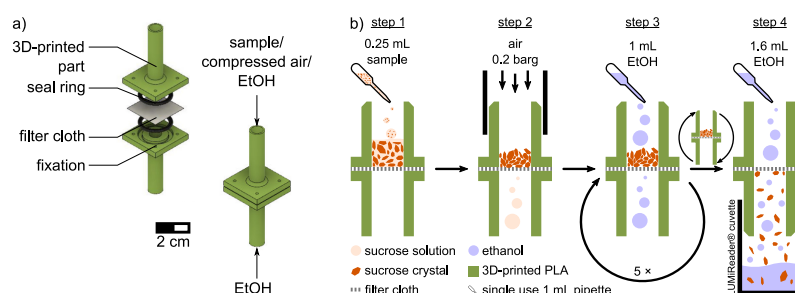

Figure S5. (a) sample preparation device 3D printed from PLA. **(b)** shows the sample washing procedure. Sucrose suspension is pipetted into one side of the device. Pressurized air and ethanol free the crystals from mother liquor. The device is then turned upside down and the crystals are flushed back into a cuvette with ethanol for analysis.
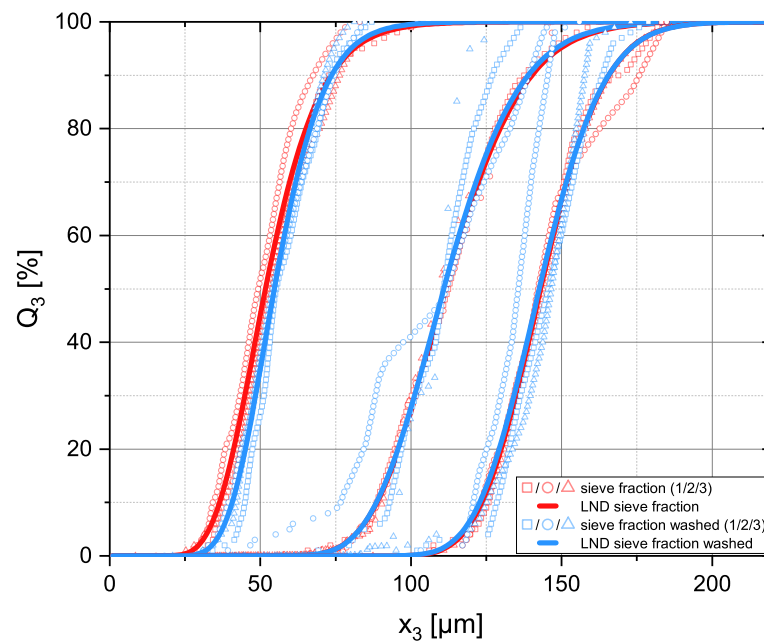
Figure S6. Cumulative and volumetric crystal size distribution of three different sieve size fractions of sucrose (63 µm-90 µm; 90 µm-125 µm; 125 µm-180 µm) analyzed with the LUMiReader®. In red are the distributions of sieved crystals directly suspended in EtOH. In blue are the distributions of crystals that were suspended in saturated sucrose solution (at room temperature) and subjected to the described washing procedure. The lines are LNDs calculated from the triple experiments.

The results of this analysis can be seen in Figure S6. The lognormal distribution (LND) has been calculated according to:

$$Q_3 = \frac{1}{2}\left[1 + erf\left(\frac{\ln\frac{x}{x_{50,3}}}{\sqrt{2}\cdot\sigma_{\mathrm{LND}}}\right)\right] \tag{1}$$

The parameter σ_{LND} has been determined with a least-squares fitting method applied to each experimental dataset of the study. Since the deviations between the LNDs of the experiments with and without washing are in a justifiable range it is concluded that the washing step has only a negligible influence on the results of the analysis. The negligible effect allows a fast analysis of CSDs and room temperature independent measurement during the experiment.
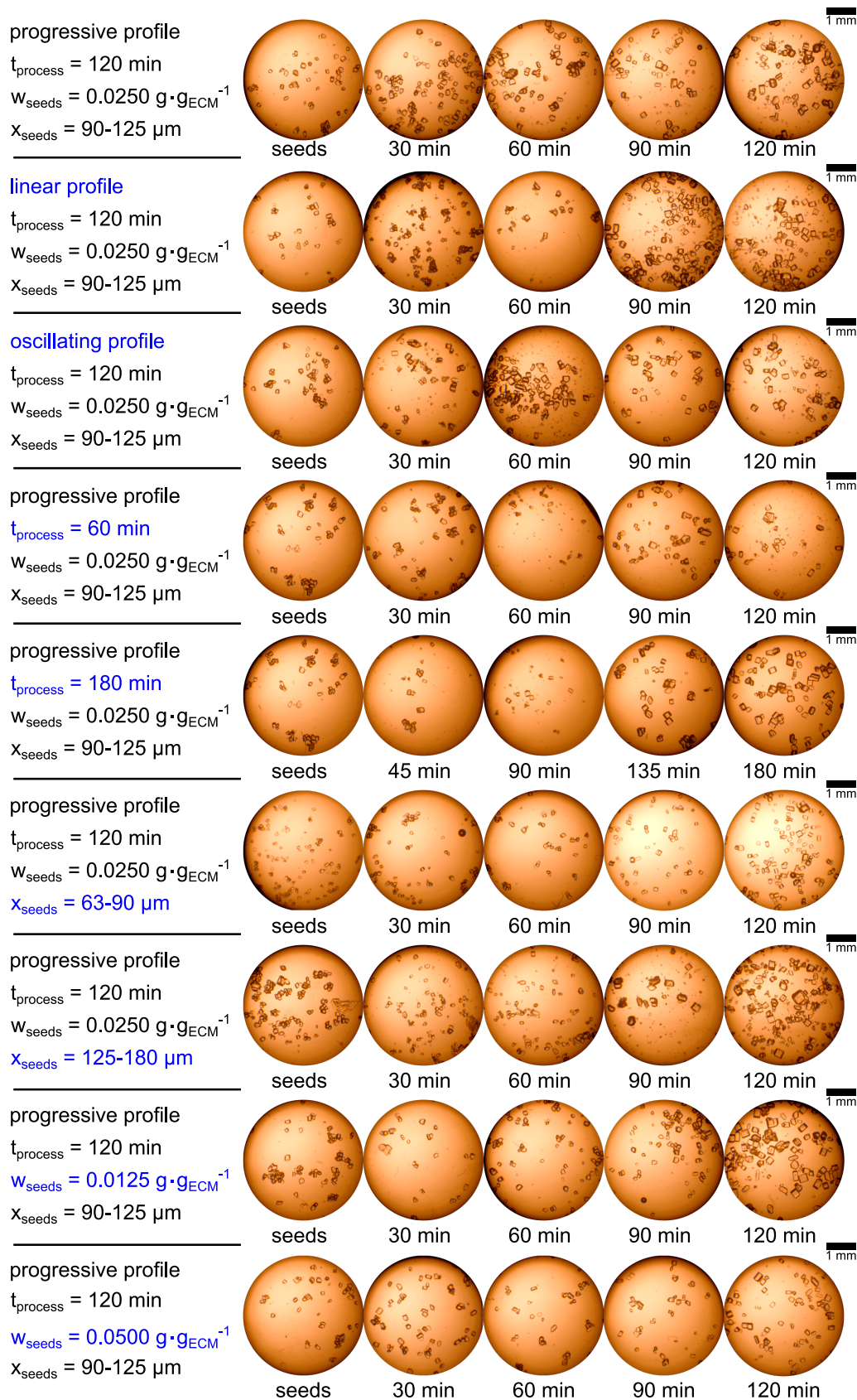
6. Supplementary Information: Crystal Images

progressive profile
$t_{process}$ = 120 min
w_{seeds} = 0.0250 g·g_{ECM}^{-1}
x_{seeds} = 90-125 µm

seeds | 30 min | 60 min | 90 min | 120 min

linear profile
$t_{process}$ = 120 min
w_{seeds} = 0.0250 g·g_{ECM}^{-1}
x_{seeds} = 90-125 µm

seeds | 30 min | 60 min | 90 min | 120 min

oscillating profile
$t_{process}$ = 120 min
w_{seeds} = 0.0250 g·g_{ECM}^{-1}
x_{seeds} = 90-125 µm

seeds | 30 min | 60 min | 90 min | 120 min

progressive profile
$t_{process}$ = 60 min
w_{seeds} = 0.0250 g·g_{ECM}^{-1}
x_{seeds} = 90-125 µm

seeds | 30 min | 60 min | 90 min | 120 min

progressive profile
$t_{process}$ = 180 min
w_{seeds} = 0.0250 g·g_{ECM}^{-1}
x_{seeds} = 90-125 µm

seeds | 45 min | 90 min | 135 min | 180 min

progressive profile
$t_{process}$ = 120 min
w_{seeds} = 0.0250 g·g_{ECM}^{-1}
x_{seeds} = 63-90 µm

seeds | 30 min | 60 min | 90 min | 120 min

progressive profile
$t_{process}$ = 120 min
w_{seeds} = 0.0250 g·g_{ECM}^{-1}
x_{seeds} = 125-180 µm

seeds | 30 min | 60 min | 90 min | 120 min

progressive profile
$t_{process}$ = 120 min
w_{seeds} = 0.0125 g·g_{ECM}^{-1}
x_{seeds} = 90-125 µm

seeds | 30 min | 60 min | 90 min | 120 min

progressive profile
$t_{process}$ = 120 min
w_{seeds} = 0.0500 g·g_{ECM}^{-1}
x_{seeds} = 90-125 µm

seeds | 30 min | 60 min | 90 min | 120 min

Figure S7. Images of crystals for the different experiments. Varied parameter is indicated in blue.

7. Supplementary Information: Raw data

Table S1. Results as raw data obtained from the experiments. Each column corresponds to one set of experiments (triplets).

profile	[-]	prog. ↓	lin. ↓	oscil. ↓	prog. ↓	prog. ↓	prog. ↓	prog. ↓	prog. ↓	prog. ↓
$t_{process}$	[min]	120	120	120	60	180	120	120	120	120
$x_{seed\ size}$	[µm]	90-125	90-125	90-125	90-125	90-125	63-90	125-180	90-125	90-125
w_{seeds}	[g·g$_{ECM}^{-1}$]	0.025	0.025	0.025	0.025	0.025	0.025	0.025	0.0125	0.05
$x_{1,3}$	[µm]	100.10	72.48	103.97	61.16	117.34	84.77	85.65	132.00	92.33
stdev	[µm]	12.91	4.80	3.77	19.04	3.39	4.90	3.78	6.00	6.66
stdev$_{rel.}$	[%]	12.90	6.62	3.63	31.13	2.89	5.78	4.41	4.55	7.22
$x_{10,3}$	[µm]	120.70	88.67	127.70	86.59	131.36	99.48	105.00	140.60	115.00
stdev	[µm]	5.72	1.59	6.13	18.19	2.03	11.63	2.72	8.20	1.82
stdev$_{rel.}$	[%]	4.74	1.80	4.80	21.00	1.54	11.69	2.59	5.83	1.59
$x_{50,3}$	[µm]	157.60	132.40	151.57	132.53	172.59	151.5	151.1	167.05	144.20
stdev	[µm]	2.03	0.86	2.69	1.76	1.51	3.40	1.93	0.15	0.85
stdev$_{rel.}$	[%]	1.29	0.65	1.78	1.32	0.87	2.24	1.28	0.09	0.59
$x_{90,3}$	[µm]	174.63	157.60	170.10	146.40	187.34	160.53	171.83	187.70	168.47
stdev	[µm]	5.85	6.75	4.14	6.70	5.88	10.02	1.72	3.30	9.00
stdev$_{rel.}$	[%]	3.35	4.28	2.44	4.58	3.14	6.24	1.00	1.76	5.34
$x_{99,3}$	[µm]	179.67	162.83	174.60	162.13	191.04	185.03	196.67	191.70	173.37
stdev	[µm]	9.02	9.50	5.46	15.74	7.92	16.49	4.71	3.30	9.69
stdev$_{rel.}$	[%]	5.02	5.84	3.13	9.71	4.15	8.91	2.40	1.72	5.59
span	[-]	0.34	0.52	0.28	0.45	0.32	0.40	0.44	0.28	0.37
stdev	[-]	0.07	0.04	0.04	0.11	0.04	0.09	0.01	0.07	0.07
stdev$_{rel.}$	[%]	19.66	6.98	15.57	23.60	13.62	23.28	3.16	24.50	18.68
IQR$_{90,10}$	[µm]	53.93	68.93	42.40	59.51	55.98	61.05	66.83	31.40	53.47
stdev	[µm]	10.51	5.19	6.13	13.56	7.18	14.37	2.08	24.11	10.03
stdev$_{rel.}$	[%]	19.48	7.53	14.45	22.78	12.83	23.54	3.12	76.77	18.76
Yield$_{rel.}$	[%]	90.43	95.50	96.58	58.25	97.77	97.56	60.54	96.98	90.80
stdev	[%]	1.32	1.74	1.02	1.97	1.20	1.90	3.90	1.03	2.36

References

1. Löbnitz, L. *Auslegung des Separationsprozesses und Entwicklung neuer Verfahrenskonzepte zur integrierten Produktion und Separation kristalliner Aminosäuren*; Karlsruher Institut für Technologie: Karlsruhe, Germany, 2020.
2. Dobler, T.; Buchheiser, S.; Gleiß, M.; Nirschl, H. Development and Commissioning of a Small-Scale, Modular and Integrated Plant for the Quasi-Continuous Production of Crystalline Particles. *Processes* **2021**, *9*, 663. doi:10.3390/pr9040663.
3. Chianese, A., Fines Removal. In *Industrial Crystallization Process Monitoring and Control*; John Wiley & Sons, Ltd, 2012; chapter 15, pp. 175–184. doi:10.1002/9783527645206.ch15.
4. Bouchard, A.; Hofland, G.W.; Witkamp, G.J. Properties of Sugar, Polyol, and Polysaccharide Water−Ethanol Solutions. *J. Chem. Eng. Data* **2007**, *52*, 1838–1842. doi:10.1021/je700190m.